Polym. Bull. (2015) 72:103–116
DOI 10.1007/s00289-014-1262-7

ORIGINAL PAPER

Crystallization of polylactide during impregnation with liquid CO_2

Christopher J. G. Plummer · Yoon Yonghoon · Léo Garin · Jan-Anders E. Månson

Received: 5 August 2014 / Revised: 17 September 2014 / Accepted: 13 October 2014 /
Published online: 25 October 2014

Abstract The evolution of the morphology and degree of crystallinity was investigated postmortem in initially amorphous specimens of a commercial poly(DL-lactide) with a relatively low D-lactide content, after different immersion times in liquid CO_2 at 10 °C and 5 MPa. Relatively high concentrations of CO_2 induced a crystalline phase that remained stable at room temperature after desorption of the CO_2, but was distinct from those generally associated with melt crystallization of polylactides (PLA), as demonstrated by transmission electron microscopy and wide-angle X-ray diffraction, consistent with previous observations. Crystallinity developed at the surface of the specimens within relatively short times compared with those necessary for the overall CO_2 content to reach saturation, resulting in a well-defined semicrystalline layer, whose thickness increased with immersion time. This behaviour was argued to be consistent with the existence of a well-defined diffusion front, associated with a step-like CO_2 concentration gradient that reflected a strong increase in the diffusivity of the CO_2 with the local CO_2 content. Crystallization led to a reduction in both the rate of CO_2 uptake and the CO_2 concentration at saturation compared with that observed for a poly(DL-lactide) with a significantly higher D-lactide content and little tendency to crystallize in the presence of liquid CO_2. Assuming the CO_2 to be concentrated in the amorphous regions of semicrystalline PLA, a simple model for non-linear Fickian diffusion based on data from previous desorption measurements was used to show that diffusion through the semicrystalline surface layer should dominate impregnation kinetics in initially amorphous specimens that undergo rapid crystallization above a certain critical CO_2 concentration, consistent with the observed rates of CO_2 uptake.

C. J. G. Plummer (✉) · Y. Yonghoon · L. Garin · J.-A. E. Månson
Laboratoire de Technologie des Composites et Polymères (LTC),
Ecole Polytechnique Fédérale de Lausanne (EPFL), Station 12,
1015 Lausanne, Switzerland
e-mail: christopher.plummer@epfl.ch

Keywords Polylactide · Diffusion · Crystallization · CO_2 · TEM · WAXD

Introduction

Polylactide (PLA) is a generic term for aliphatic polyesters derived from L- and D-lactides, whose degree of crystallinity may vary considerably depending on processing conditions and the L to D ratio [1]. There has been considerable recent effort to produce PLA-based foams using carbon dioxide (CO_2) as a physical blowing agent, e.g. for biomedical applications and as an alternative to expanded polystyrene for low-density packaging [2–5]. Introduction of CO_2 into the PLA generally involves compression of the former, under which conditions it may be in either the liquid state or the supercritical state depending on the temperature, T, and pressure (triple point −56.4 °C, 518 kPa, critical point 31.1 °C, 7.39 MPa). While supercritical CO_2 processing is widely used to produce foams in situ in the autoclave by controlled depressurization [5], liquid CO_2 processing has the advantage that it may be carried out at relatively low T, facilitating the preparation of high-density foam precursors that are sufficiently stable on removal from the autoclave to permit their use in a separate foaming operation [6–8]. However, the CO_2 contents of up to 0.43 g/g (mass of CO_2 per unit mass of PLA) that may be achieved by liquid CO_2 processing of nominally amorphous grades of poly(DL-lactide) (PDLLA) result in a decrease in the glass transition temperature, T_g, from its nominal value of about 60 °C to well below ambient temperature [2]. If fully stable precursors are required, it is therefore important to control the overall levels of CO_2, e.g. by allowing the CO_2 to partially desorb at relatively low temperatures [6, 8]. A further concern is that PDLLA with relatively low D-lactide contents may undergo significant cold crystallization at high CO_2 concentrations because of the depression in T_g [8–10]. While such crystallization is expected to contribute to the stability of the precursors, it may also modify their foaming characteristics in the temperature range immediately above T_g. This is of particular relevance to our current efforts to use PLA/CO_2 as a solid precursor free of volatile organic compounds (VOC) for the production of foam-core sandwich structures using a modified press-forming process, in which water vapour plays an important role in heat transfer. The aim of the present work has therefore been: (1) to investigate morphological development during sorption of liquid CO_2 by a commercial PDLLA with a low D-lactide content that crystallizes readily on annealing above T_g or during slow cooling from the melt; (2) to examine the consequences of CO_2-induced crystallization for the sorption process.

Experimental

Nominally semicrystalline PDLLA containing 1.4 % D-lactide was obtained from NatureWorks LLC in pellet form. T_g of the as-received pellets was determined from differential scanning calorimetry (DSC, TA Instruments Q2000) heating scans at

10 K/min to be 60 °C and the melting temperature, T_m, was about 170 °C. 99.9 % pure CO_2 was obtained from Carbagas AG.

The PLA pellets were compression moulded to form 1-mm-thick discs with a diameter of 20 mm using a hot press (Fontijne TP 50 with 255 × 255 mm^2 heating platens) after overnight drying at 35 °C under vacuum. The pellets were placed between polyimide release films in a stainless steel mould and conditioned in the press at 180 °C for 5 min. A nominal hydraulic force of 6 kN (equivalent to a mould pressure of 0.25 MPa) was then applied at 180 °C for a further 5 min, after which the press platens were cooled under pressure to below 40 °C over a period of ~10 min, using the integrated water cooling system. Specimens produced under these conditions were shown by DSC heating scans at 10 K/min to be highly amorphous, but with a cold crystallization endotherm starting at about 100 °C.

Impregnation with liquid CO_2 was carried out at 5 MPa and 10 °C for various times using a high-pressure chamber (Autoclave France) equipped with a mechanical cooling system. After depressurization at ~0.01 MPa/s, the specimens were weighed to estimate the total mass uptake of CO_2. The CO_2 was then allowed to desorb at 10 °C for 1 h followed by a minimum of 1 week at ambient temperature prior to all subsequent heat treatments and measurements. These conditions were shown from previous investigations of desorption kinetics to be sufficient to reduce the CO_2 to negligible levels [8].

For morphological characterization, the specimens were sectioned at room temperature using a Reichert-Jung Ultracut-E ultramicrotome equipped with a diamond knife (Diatome). Cross-sections of ~2 μm in thickness were observed in transmitted light using an optical microscope (Olympus OM2) equipped with crossed polarizers. Sections of ~50 nm in thickness were prepared for transmission electron microscopy (TEM, Tecnai Spirit BioTWIN) from specimens stained by exposure to RuO_4 vapour overnight, and observed in bright field at 80 kV. Wide-angle X-ray diffraction (WAXD, Brucker D8 Discover powder diffractometer, Cu Kα, $\lambda = 1.54$ Å) measurements were carried out in reflection mode.

Results and discussion

Morphological development during immersion in liquid CO_2

As shown in Fig. 1a, specimens impregnated for relatively short times, t_{imp}, in liquid CO_2 at 10 °C showed a well-defined, uniform, but weakly birefringent layer, extending to a constant depth from both surfaces, with no clear fine structure when observed in the optical microscope. The core regions of these specimens showed no birefringence. In Fig. 2, estimates of the volume fraction corresponding to the birefringent layers from optical microscopy are compared with $X(t)$, the measured mass uptake of CO_2 expressed in g of CO_2 per g of PLA, normalized with respect to the mass uptake of CO_2 at saturation, c_o (estimated to be 0.29 g/g), which was reached for t_{imp} greater than about 3 h. While there was considerable experimental scatter for short t_{imp}, and t_{imp} itself was associated with an uncertainty of the order of 1 min (the time necessary to reach steady-state conditions in the autoclave), the

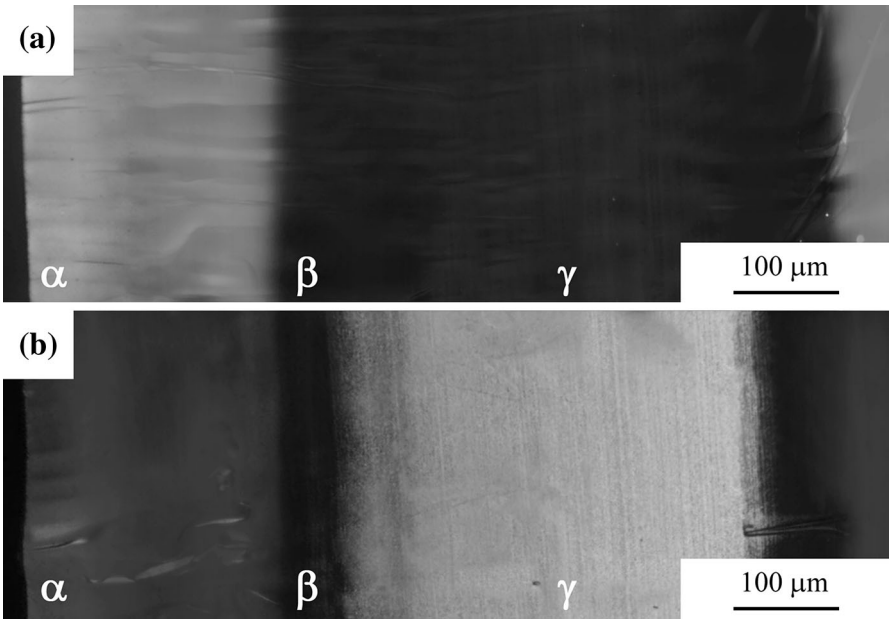

Fig. 1 Optical micrographs between crossed polarizers of **a** a semi-thin cross-section taken from a specimen held in liquid CO_2 at 10 °C for 10 min, after desorption of the CO_2, **b** a semi-thin cross-section from the same specimen and subsequently heated to 130 °C at 20 K/min using a hot stage. α, β and γ indicate the approximate positions of the specimen surface, the limit of the birefringent surface layer and the midpoint of the specimen respectively

results shown in Fig. 2 suggested the thickness of the birefringent layer to be approximately proportional to the CO_2 uptake throughout the impregnation process.

Figure 3 shows TEM micrographs of the morphology of specimens crystallized in CO_2. Although RuO_4 is known to be effective as a stain for semicrystalline PLA [11], the morphology corresponding to the birefringent regions of the specimens was poorly defined, consistent with the lack of structure in the optical images, and the broadness of the Bragg peaks in the WAXD measurements (see below). There was nevertheless some suggestion from the TEM micrographs that a lamellar texture with a lamellar thickness of roughly 10 nm was already established locally after short t_{imp}.

Figure 4 and Table 1 give results from DSC heating scans at 20 K/min on samples of $\sim$5 mg in mass taken through the whole thickness of the impregnated specimens after desorption of the CO_2. T_g showed little systematic variation for long t_{imp}, remaining at about 62 °C under these measurement conditions, but for relatively short t_{imp}, T_g increased somewhat to about 65 °C, and was associated with a marked endothermic peak, effects that were attributed to physical ageing. The as-moulded PLA specimens did not show an exothermic peak at T_g, indicating the physical ageing to have taken place during impregnation and/or desorption. The as-moulded specimens were also initially highly amorphous, as mentioned in the experimental section, and crystallization during DSC heating and cooling cycles

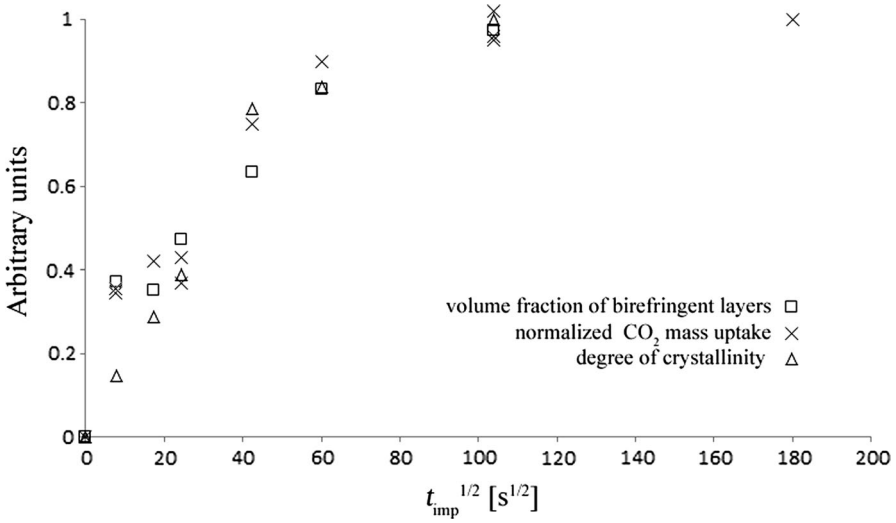

Fig. 2 The influence of impregnation time, t_{imp}, on: the estimated volume fraction of the birefringent layers observed by optical microscopy; the mass uptake of CO_2 normalized with respect to its value at saturation (0.29 g/g); the relative degree of crystallinity after desorption of the CO_2, defined as the overall melting enthalpy (in J/g) determined from DSC heating scans, normalized with respect to its limiting value after long t_{imp} (estimated to be 32 J/g)

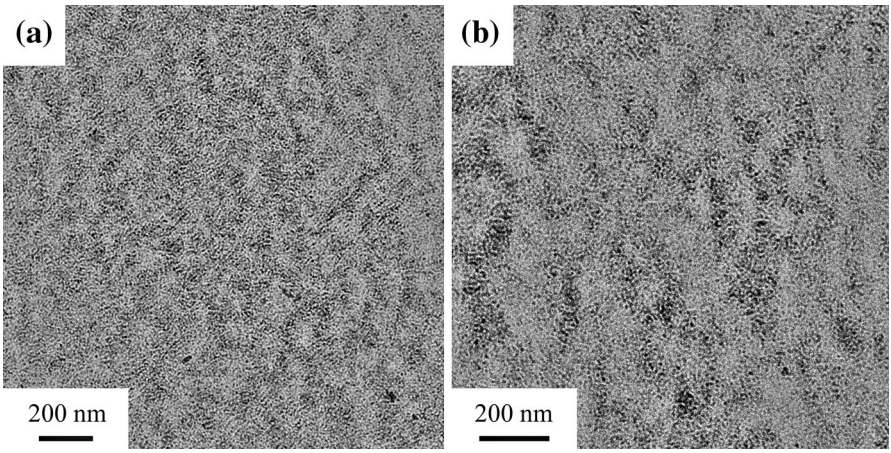

Fig. 3 TEM micrographs of RuO_4-stained sections taken from the birefringent layers in specimens exposed to liquid CO_2 at 10 °C for **a** 5 min and **b** 3 h, after desorption of the CO_2

was suppressed at scanning rates of 20 K/min. However, significant crystallinity was observed in the impregnated specimens for all the t_{imp} considered. The qualitative behaviour was similar in each case: a broad exothermic peak appeared as T increased above T_g, followed by a marked endotherm, with a peak temperature of between 168 and 173 °C, depending on t_{imp}. A heating rate of 20 K/min ensured the

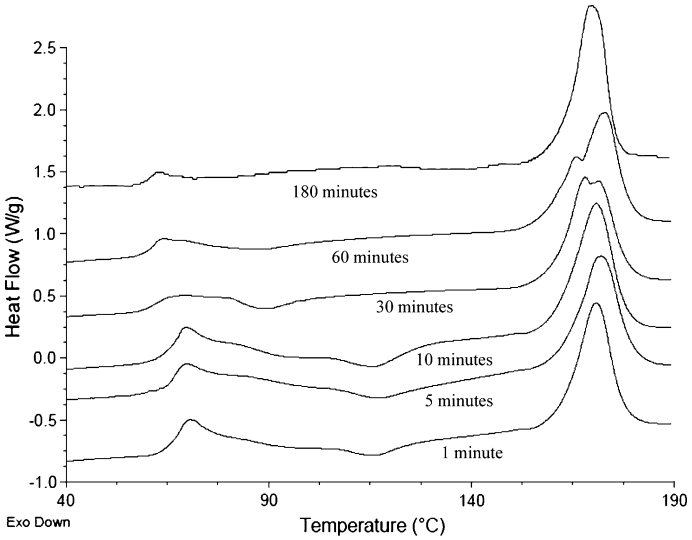

Fig. 4 DSC first heating scans at 20 K/min for the different t_{imp} indicated

Table 1 Summary of data from DSC first heating scans at 20 K/min for the different t_{imp} indicated

t_{imp} (min)	T_g (°C)	Exotherm peak (°C)	Upper melting peak (°C)	Lower melting peak (°C)	Melting enthalpy (J/g)
1	65	116	170	–	4.69
5	65	117	171	–	9.24
10	65	116	171	–	12.5
30	63	90	171	168	25.2
60	62	87	172	166	26.9
180	62	–	169	–	32.0

onset of the exotherm to be sufficiently well separated from the glass transition and the associated endotherm to allow unambiguous definition of a linear baseline from which the overall enthalpy change during the scans could be determined, regardless of t_{imp} (this was not true of lower heating rates, but results obtained at 10 K/min were generally consistent with those shown here). The melting enthalpy tended to about 32 J/g after long t_{imp} (3 h or more), and, as seen from Fig. 2, the enthalpy change obtained at intermediate t_{imp} ($t_{imp} > 5$ min) normalized with respect to this limiting value were broadly similar to the normalized degree of CO_2 uptake at the same t_{imp}. On the other hand, for shorter t_{imp}, the normalized melting enthalpies were relatively low, suggesting a few minutes to be necessary for the degree of crystallinity to reach its limiting value in regions of high CO_2 content.

The peak temperature of the main exotherm in the DSC heating scans was close to 116 °C for low t_{imp}, which is in the same temperature range as the peak spherulite

growth rates determined from hot-stage microscopy of specimens crystallized from the melt, and the maximum crystallization rates in isothermal DSC measurements. It may be inferred, therefore, that these exotherms corresponded mainly to crystallization of regions of the specimens that remained substantially amorphous during impregnation, although the nucleation rate was presumably higher than in the as-moulded specimens. Corroborating evidence for this was provided by hot-stage optical microscopy of sections from partially impregnated specimens (Fig. 1b), which showed the core to develop a fine spherulitic texture during heating. As the original CO_2 content approached saturation, the DSC exotherm weakened, and its peak shifted to lower temperatures, e.g. about 87 °C for $t_{imp} = 1$ h. Moreover, the form of the onset of the exotherm appeared similar in all the specimens, possibly reflecting the existence of a "transition zone" of enhanced nucleation between the birefringent layers and the amorphous core.

The peak temperature of the main melting endotherm initially changed little with increasing t_{imp}, remaining at between 170 and 171 °C. For longer t_{imp}, however, two melting peaks were observed; the upper peak temperature increasing to about 172 °C as t_{imp} increased to 1 h, while the temperature of the lower melting peak decreased from 168 to 166 °C as t_{imp} increased from 0.5 to 1 h. Finally, in saturated specimens (t_{imp} of 3 h or more), a single melting peak was observed at about 169 °C. The main DSC melting peak at comparable scanning rates for PLA crystallized by heating from the glassy state or for specimens crystallized isothermally at temperatures below about 125 °C generally results from reorganization during the scan, and, as will be discussed below, there was direct evidence from WAXD for a crystal–crystal transformation during heating of specimens crystallized in liquid CO_2. Even so, the relatively low final melting temperature of these latter was assumed to reflect an initial state of reduced crystalline order.

To obtain further insight into the rate of crystallization in liquid CO_2, WAXD was used to investigate the evolution of the crystalline morphology at the specimen surfaces. Figure 5 gives results from surface scans for different t_{imp}. The as-moulded specimens showed amorphous scattering with a first-order maximum at 2θ of about 16°. On the other hand, for $t_{imp} = 1$ min, a broad Bragg peak was visible at 2θ in the range 15.5°–15.9°, and an additional peak at 2θ of about 32.5° (weak peaks were also present in the vicinity of 18°). While it was not possible to estimate an absolute degree of crystallinity from the WAXD curves under the present conditions, these peaks appeared better defined for $t_{imp} = 5$ min, but showed little change for longer t_{imp}, again implying crystallization to take place on a time scale of a few minutes, i.e. very much shorter than the overall saturation time (cf. the results in Fig. 2).

Similar WAXD patterns have been reported previously for PLA crystallized under high-pressure CO_2 in this temperature range, and are distinct from those observed in specimens cold crystallized above T_g in the absence of CO_2 or crystallized from the melt [9, 10, 12, 13]. In the present case, isothermal crystallization of the as-moulded specimens at 110 °C resulted in sharp Bragg peaks at 2θ of 14.5°, 16.5°, 18.8° and 22.2° (Fig. 6d), characteristic of the orthorhombic α modification, i.e. a pseudo-hexagonal arrangement of 10_7 helices with a repeat distance in the c direction of 28.8 Å [14]. The most intense peak at 16.5°

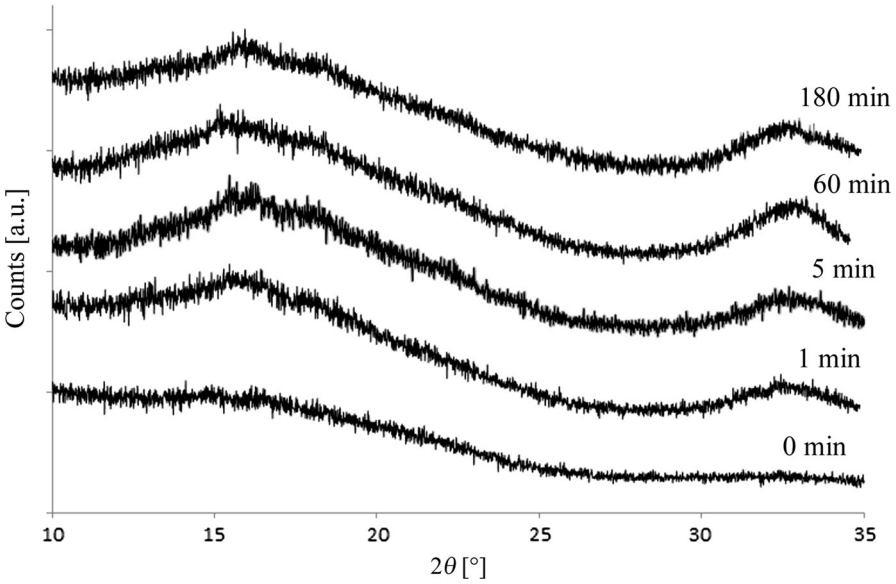

Fig. 5 WAXD scans from the surface of specimens exposed to liquid CO_2 at 10 °C for the different times, t_{imp}, indicated

corresponded to a superposition of the (1 1 0) and (2 0 0) reflections, with $d = 5.37$ Å. This is slightly larger than typical published values for the PLLA homopolymer [14, 15], but significantly less than the values of 5.6–5.7 Å associated with the peak at $2\theta = 15.5°$–$15.9°$ observed in the specimens crystallized in liquid CO_2. Assuming a pseudo-hexagonal arrangement for these latter, the area of the basal plane of the unit cell was $\sim$12 % greater than for the α modification. If the spacing of 2.75 ± 0.5 Å inferred from the high-angle peak about 32.5° is taken to correspond to the mean intrachain atomic spacing in the c direction (cf. the 2.88 Å spacing of the (0 0 1 0) planes in the α modification), the volume of the unit cell is estimated to be some 8 % greater than for the α modification. It follows that CO_2 molecules may have been trapped within the crystalline phase during its formation, as has been suggested elsewhere [10], so that the disorder apparent from the WAXS results may reflect not only the initial state of the crystalline phase, but also modifications induced by desorption. (It would be of interest in this respect to carry out further WAXS measurements in transmission prior to complete desorption of the CO_2).

When as-moulded specimens were annealed at 80 °C, peaks were visible at 2θ of 16.4° and 18.7°, but the peaks at 14.5° and 22.2° characteristic of the α modification were absent, indicating the more disordered α′ modification, generally observed at relatively low crystallization temperatures, to dominate under these conditions [16]. Figure 6 shows the effect of annealing for 0.5 h at various temperatures on specimens crystallized by exposure to liquid CO_2 at 10 °C. In this case, a transition to the α modification was observed at annealing temperatures of both 80 and

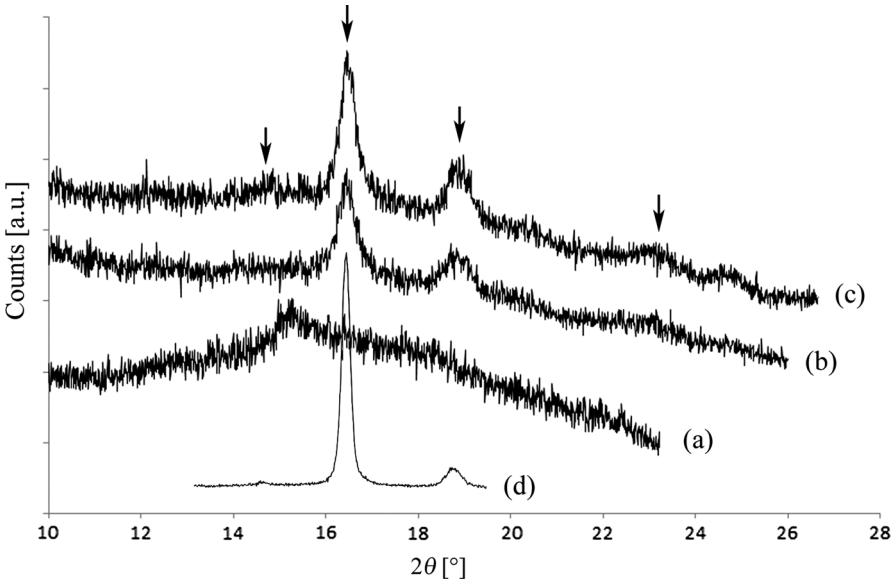

Fig. 6 WAXD scans from the surface of initially amorphous specimens exposed to liquid CO_2 at 10 °C for 30 min and annealed for 30 min at *a* 60 and *b* 80 and *c* 100 °C after desorption of the CO_2 (the *arrows* indicate the positions of the principal Bragg peaks corresponding to the α modification). *d* shows data for a the same grade of PLA crystallized isothermally at 110 °C for comparison (not to the same scale)

100 °C, although the relatively broad Bragg peaks indicated reduced crystallite dimensions. On the other hand, the phase induced by exposure to liquid CO_2 remained relatively stable during annealing at 60 °C.

Consequences for rate of CO_2 uptake

Previous investigations of CO_2 desorption rates from specimens of the same grade of PLA impregnated under in liquid CO_2 at 10 °C have indicated the rate of diffusion of the CO_2 to be strongly concentration dependent, as expected, given that high concentrations of CO_2 are expected to lead to a significant reduction in T_g [8, 17]. Assuming Fickian diffusion, the dependence of the diffusion coefficient, D, on the CO_2 concentration, c, was modelled over the whole range of c from 0 to c_o, using

$$D(c) = D_0 \exp(Ac), \tag{1}$$

where D_0 and A are empirical fitting constants (D_0 is the limiting value of D at zero CO_2 concentration) [18–20]. Desorption data obtained from fully impregnated specimens at 10 °C implied A to be about 23, from which it was shown that sorption under the same conditions, i.e. into a specimen with an equivalent structure, should be characterized by a step-like concentration profile that gradually advances into the specimen, i.e. qualitatively similar behaviour to "case II" diffusion, assuming D to show the same dependence on c as for desorption [8, 21, 22].

This approach takes into account neither the effect of swelling on the specimen dimensions, nor the possibility of non-Fickian effects, and indeed the assumption of a path-independent diffusion coefficient is highly questionable, particularly given the possibility of entrapment of CO_2 molecules by the crystalline phase when it first forms. However, the approximate superposition of the data in Fig. 2 is at least consistent with the existence of a step-like diffusion front during diffusion of CO_2 into an initially amorphous specimen. The sharp boundary observed between the birefringent and non-birefringent regions of partially impregnated specimens implies a steep concentration gradient on the scale of the micrographs. It is also reasonable to assume from the WAXD results that crystallization develops within a few minutes for c greater than some critical value (i.e. sufficient to reduce T_g to well below 10 °C, in the present case). Given that the onset of cold crystallization in PLA is typically observed at temperatures about 10 °C greater than the nominal T_g in DSC heating scans, the critical concentration, c_c, is assumed to be of the order of, or greater than 0.17 g/g, i.e. sufficient to reduce T_g to 0 °C [8, 17].

Under these conditions, the overall degree of crystallinity is expected to be at least roughly correlated with the position of diffusion front after relatively long diffusion times, consistent with Fig. 2. Moreover, the internal morphologies of partially impregnated specimens foamed by heating to 100 °C after depressurization and conditioning at 10 °C in order to obtain a relatively uniform CO_2 concentration profile, have been argued previously to reflect the presence of relatively highly crystalline regions at the specimen surfaces, in which foaming was substantially suppressed, and whose extent was consistent with approximate predictions of the position of the diffusion front immediately after impregnation [8]. It should nevertheless be borne in mind that during desorption, CO_2 diffuses into regions of the specimen beyond the original diffusion front, albeit at reduced concentrations. This may account for the transition zone referred to earlier, as well as the enhanced nucleation rates and physical ageing in the cores of partly impregnated specimens.

One limiting scenario that emerges from this discussion is one of a crystallization front and a step-like diffusion front that advance almost simultaneously into the initially amorphous specimens. In an effort to understand how this affects diffusion rates, Eq. 1 was assumed to describe $D(c)$ in a homogenous material. For large A, and t_{imp} shorter than the time for the diffusion front to reach the centre of an infinitely wide specimen of thickness l,

$$\frac{X(t_{imp})}{c_o} = F(Ac_o)\frac{\sqrt{D_0 t_{imp}}}{l}, \tag{2}$$

where $F(Ac_o)$ is a function of Ac_o only [20]. To simplify further, it was also assumed: (1) that crystallinity influences D_0 through a tortuosity factor, $\tau \approx \phi_a^{-n}$, where ϕ_a is amorphous volume fraction, so that D_0 is replaced by D_0/τ in semicrystalline specimens [23]; (2) that the CO_2 concentration in the amorphous regions of a semicrystalline specimen is equal to $c/(1-\chi)$ for an overall concentration c, where χ is the mass fraction of the crystalline material (i.e. it was assumed that there is no CO_2 in the crystalline regions). The diffusion coefficient is then

$$D(c,\chi) = \frac{D_0}{\tau}\exp\left(\frac{Ac}{1-\chi}\right). \tag{3}$$

Because the effective value of A in Eq. 3 is $A/(1-\chi)$, and the effective saturation concentration is $c_o(1-\chi)$, the factor $F(Ac_o)$ in Eq. 2 is independent of χ, and the normalized rate of CO_2 uptake is merely reduced by a factor $\tau^{-1/2}$.

To model simultaneous diffusion and crystallization numerically, the surface concentration was assumed to be equal to $c_o(1-\chi)$ and that crystallization takes place instantaneously when $c \geq c_c$, so that

$$\left.\begin{aligned} D(c \geq c_c) &= \frac{D_0}{\tau}\exp\left(\frac{Ac}{1-\chi}\right) \\ D(c < c_c) &= D_0\exp(Ac) \end{aligned}\right\} \tag{4}$$

Figure 7 shows predictions of the CO_2 uptake for infinitely wide 1-mm-thick specimens and various c_c, with $A/(1-\chi) = 23$, $c_o(1-\chi) = 0.29$ g/g and $D_0/\tau = 1.8 \times 10^{-13}$ m^2/s, as estimated previously from desorption measurements on fully saturated specimens at 10 °C [8]. χ was taken to be 0.34, assuming the enthalpy of fusion of the crystalline phase to be 93.1 J/g, a value widely assumed for melt-crystallized PLA (although it is not clear that it is appropriate to crystallization in CO_2) [24]. Also shown for comparison are predictions for fully amorphous PLA, i.e. for $\chi = 0$, assuming $\tau = 2$ as in previous work, along with data for the CO_2 uptake in the initially amorphous specimens of the PLA grade under consideration here, and for a fully amorphous grade of PLA [8].

For fully amorphous and fully crystallized specimens, the predicted overall CO_2 content increased linearly with $t_{imp}^{1/2}$ up to about 80 % of the surface concentration,

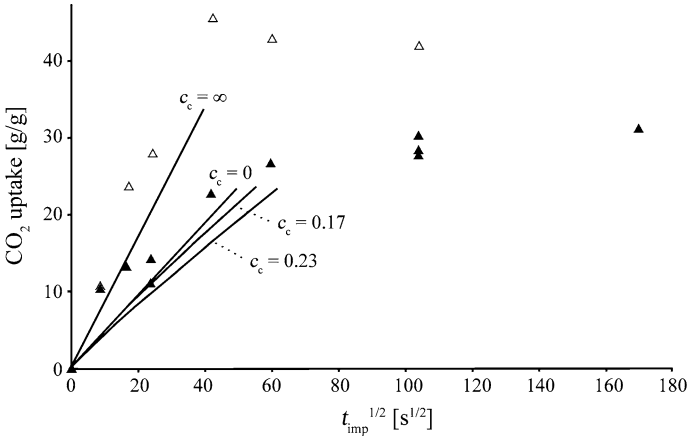

Fig. 7 Predicted CO_2 uptake at 5 MPa and 10 °C as a function of t_{imp} for infinitely wide 1-mm-thick specimens and various c_c as indicated, along with data for the CO_2 uptake in the initially amorphous specimens of the crystallizable PLA grade under consideration here (*filled triangles*), and for a fully amorphous grade of PLA (*open triangles*)

beyond which the opposing diffusion fronts overlapped, and Eq. 1 was no longer valid. However, as seen from Fig. 7, numerical calculations based on Eq. 4 for initially amorphous specimens that undergo instantaneous crystallization when $c > c_c$, implied the impregnation rate at relatively long t_{imp} to decrease slightly with respect to the predictions for fully crystallized PLA, particularly as c_c approached the surface concentration, $c_o(1 - \chi)$. Initially, when the concentration gradients are large, the overall diffusion rates are controlled by the behaviour at high c, for which the specimens are assumed to have crystallized, so that the behaviour is similar to that of a fully crystallized specimen. The present model nevertheless implies reduced diffusion rates in the absence of crystallization for a given c. This is because the effective concentration in the amorphous regions of a semicrystalline specimen is greater by a factor $1/(1 - \chi)$ than in a fully amorphous specimen, and the exponential dependence of the diffusion coefficient on concentration dominates the geometrical barrier effect of the crystalline phase as expressed by τ. This leads to a decrease in the rate of CO_2 uptake as the concentration gradients decrease.

Bearing in mind the considerable experimental scatter, the data in Fig. 7 suggested significant deviations from the model predictions at low t_{imp}, where the rates of CO_2 appeared similar for the fully amorphous PLA and initially amorphous specimens of the crystallisable PLA. The rate of CO_2 uptake in these latter nevertheless diminished significantly as t_{imp} increased from 1 to 5 min and was roughly asymptotic to the model predictions for the fully crystallized PLA as t_{imp} increased further, i.e. significantly lower than for the fully amorphous PLA. Given that a few minutes were necessary for the degree of crystallinity to reach its limiting value at high CO_2 concentrations, this initial transient was assumed to correspond to the time necessary for establishment of the shielding effect of the crystalline regions. Indeed, prior to full crystallization at the specimen surfaces, the local CO_2 presumably reached levels comparable with those in the fully amorphous PLA, explaining the initially rapid increase in both the overall CO_2 concentration, and the thickness of the birefringent layer (cf. Fig. 2), which reached more than a third of specimen half-thickness after only 1 min.

Conclusions

The results presented here are consistent with the existence of a step-like diffusion front during diffusion of liquid CO_2 into PLA at 10 °C. For initially amorphous low D-lactide PDLLA specimens, the position of the diffusion front after a given impregnation time was shown to be associated with a step-like increase in birefringence, which was associated with CO_2-induced crystallization above a certain critical concentration of CO_2, giving rise to a crystal modification distinct from that generally observed in specimens crystallized from the melt in the absence of CO_2. The most obvious consequence of this crystallization was a significant decrease in the rate of CO_2 uptake and overall CO_2 content at saturation compared with that observed for PDLLA with a relatively high D-lactide content that showed little tendency to crystallize. This may be seen as a consequence of the establishment of physical barrier to diffusion at the specimen surface that shields

the interior from the high CO_2 concentrations associated with the immersion of fully amorphous PLA in liquid CO_2. It was demonstrated using a simplified model for a specimen that crystallizes instantaneously above some critical CO_2 concentration, that diffusion rates are expected to be dominated by the semicrystalline regions in this limit, so that the rate of CO_2 uptake by an initially amorphous specimen should be similar to that for an initially semicrystalline specimen. Indeed, it was suggested on this basis that the overall diffusion rates may even be slightly reduced in initially amorphous specimens. On the other hand, a transient regime was observed for relatively short impregnation times, in which the rate of CO_2 uptake was initially close to that observed for fully amorphous specimens, and which was argued to reflect the time necessary for establishment of the semicrystalline barrier layer at the specimen surfaces. Coupling between the local degree of crystallinity, the CO_2 content at saturation and the CO_2 content in the amorphous regions, is assumed to invalidate the assumptions inherent in the Fickian approach used to model diffusion in fully crystallized or fully amorphous PLA. Even so, the qualitative insight into the diffusion process provided by the present work is expected to contribute to efforts to optimize precursor geometries (effective specimen thickness) and impregnation conditions (time, temperature) for the CO_2 foaming of low D-lactide PDLLA at relatively low foaming temperatures (i.e. above the nominal T_g, but well below the melting range of the α phase.

Acknowledgments We are grateful to the Swiss National Science Foundation for financial support through the Program NRP 66 "Resource Wood" and the Interdisciplinary Centre for Electron Microscopy (CIME) of the EPFL for their technical support.

References

1. Garlotta D (2001) A literature review of poly(lactic acid). J Polym Environ 9:63–84
2. Parker K, Garancher J-P, Shah S, Weal S, Fernyhough A (2011) Polylactic acid (PLA) foams for packaging applications. In: Pilla S (ed) The handbook of bioplastics and biocomposites engineering applications. Wiley/Scrivener Publishing LLC, Hoboken/Salem, pp 161–175
3. Parker K, Garancher J-P, Shah S, Fernyhough A (2011) Expanded polylactic acid—an eco-friendly alternative to polystyrene foam. J Cell Plast 47:233–243
4. Barry JJA, Silva MMCG, Popov VK, Shakesheff KM, Howdle SM (2006) Supercritical carbon dioxide: putting the fizz into biomaterials. Phil Trans R Soc A 364:249–261
5. Mathieu LM, Montjovent M-O, Bourban P-E, Pioletti DP, Månson J-AE (2005) Bioresorbable composites prepared by supercritical fluid foaming. J Biomed Mater Res 75:89–97
6. Witt MRJ, Shah S (2008) Methods of manufacture of polylactic acid foams. WO 2008(093284):A1
7. Witt M, Parker K, Shah S, Anderson R (2006) A new green approach for turning PLA plastic granules into commodity foam. In: Iannace S, Park CB (eds) Proc 1st International Conference on Biofoams. Capri, Italy, pp 23–24
8. Yoon YH, Plummer CJG, Thoemen H, Månson J-AM (2014) Liquid CO_2 processing of solid polylactide foam precursors. J Cell Plast. doi:10.1177/0021955X14537662
9. Hirota S, Sato T, Tominaga Y, Asai S, Sumita M (2006) The effect of high-pressure carbon dioxide treatment on the crystallization behavior and mechanical properties of poly(L-lactic acid)/poly (methyl methacrylate) blends. Polymer 47:3954–3960
10. Marubayashi H, Akaishi S, Akasaka S, Asai S, Sumita M (2008) Crystalline structure and morphology of poly(L-lactide) formed under high-pressure CO_2. Macromolecules 41:9192–9203
11. Delabarde C, Plummer CJG, Bourban P-E, Månson J-AM (2010) Accelerated ageing and degradation in poly-L-lactide/hydroxyapatite nanocomposites. Polym Deg Stab 96:595–607

12. Mihai M, Huneault MA, Favis BD (2009) Crystallinity development in cellular poly(lactic acid) in the presence of supercritical carbon dioxide. J Appl Polym Sci 113:2920–2932
13. Zhai W, Ko Y, Wong A, Park CB (2009) A study of the crystallization, melting, and foaming behaviors of polylactic acid in compressed CO_2. Int J Mol Sci 10:5381–5397
14. De Santis P, Kovacs A (1968) Molecular conformation of poly(s-lactic acid). J Biopolym 6:299–306
15. Hoogsteen W, Postema AR, Pennings AJ, ten Brinke G, Zugenmaier P (1990) Crystal structure, conformation and morphology of solution-spun poly(L-lactide) fibers. Macromolecules 23:634–642
16. Zhang J, Duan Y, Sato H, Tsuji H, Noda I, Yan S, Ozaki Y (2005) Crystal modifications and thermal behavior of poly(L-lactic acid) revealed by infrared spectroscopy. Macromolecules 38:8012–8021
17. Chow TS (1980) Molecular interpretation of the glass transition temperature of polymer-diluent systems. Macromolecules 13:362–364
18. Crank J, Park GS (1968) Diffusion in polymers. Academic, New York
19. Zhou S, Stern SA (1989) The effect of plasticization on the transport of gases in and through glassy polymers. J Polym Sci Pol Phys 27:205–222
20. Huang J-C, Liu H, Liu Y (2006) Diffusion in polymers with concentration dependent diffusivity. Int J Polym Mater 49:15–24
21. Peterlin A (1965) Diffusion in a network with discontinuous swelling. J Polym Sci Pol Lett 3:1083–1087
22. Thomas NL, Windle AS (1981) A theory of case II diffusion. Polymer 23:529–542
23. Hedenqvist M, Gedde UW (1996) Diffusion of small-molecule penetrants in semicrystalline polymers. Prog Polym Sci 21:299–333
24. Fischer EW, Sterzel HJ, Wegner G (1973) Investigation of the structure of solution grown crystals of lactide copolymers by means of chemicals reactions. Kolloid-Zu Z Polym 251:980–990